Adsorption (2014) 20:977–985
DOI 10.1007/s10450-014-9643-7

Scale inhibitor adsorption studies in rock sandstone type

Carolina B. Veloso · Álvaro N. A. Silva · Thiago T. G. Watanabe · J. Felipe B. C. Paes · F. Murilo T. de Luna · Célio L. Cavalcante Jr.

Received: 7 July 2014 / Revised: 16 October 2014 / Accepted: 20 October 2014 / Published online: 6 November 2014

Abstract In offshore petroleum fields, the reservoir injection of seawater and produced waters, are in fact common operations with purpose to stimulate and increase the productions. However, this particular method causes the scale formation damaging the production structures. In order to prevent the formation of the aforesaid deposits, it is common to use the squeeze treatment, whereby the scale inhibitors were injected into the wellbore and may also be adsorbed or precipitated into the rock surface. In this study, the interactions between a commercial scale inhibitor and a sandstone rock were evaluated. The column experiments were performed for different feed concentrations and temperatures. The simulation models (Linear Drive Force and General Rate) were used to predict the breakthrough curves and estimate the mass transfer parameters. Whereas, isotherms were obtained from the breakthrough curves and the maximum adsorption capacity of 6.17 mg g^{-1} was determined. A remarkable agreement between the experimental data and the representation model was observed. The low diffusion coefficients, between 0.1×10^{-5} and 9.78×10^{-5} cm^2 min^{-1}, characterized this particular process as a high diffusion resistance. Regarding the desorption tests, part of the inhibitor still remained in the column. This said behavior in the squeeze treatment is expected, since the inhibitor remains in contact with the rock for a longer period, it being possible to expand the lifetime of the squeeze treatment.

C. B. Veloso · Á. N. A. Silva · T. T. G. Watanabe · J. F. B. C. Paes · F. M. T. de Luna (✉) · C. L. Cavalcante Jr.
Departamento de Engenharia Química, Grupo de Pesquisa em Separações por Adsorção – GPSA, Universidade Federal do Ceará, Campus do Pici, Bl. 709, Fortaleza, CE 60.455-900, Brazil
e-mail: murilo@gpsa.ufc.br

Keywords Adsorption · Scale inhibitor · Sandstone rock · Mass transfer · Modeling and simulation

Symbols

B	Langmuir equation parameter, affinity adsorbate/adsorbent (mL mg^{-1})
C	Bulk liquid phase concentration (mg mL^{-1})
C_{eq}	Equilibrium concentration (mg mL^{-1})
C_0	Initial concentration (mg mL^{-1})
C_p	Intra-particle liquid phase concentration (mg mL^{-1})
d_p	Average particle diameter (cm)
D_m	Molecular diffusion coefficient (cm^2 min^{-1})
D_p	Pore diffusion coefficient (cm^2 min^{-1})
D_{ax}	Axial dispersion coefficient (cm^2 min^{-1})
k_f	Film mass transfer coefficient (cm min^{-1})
K_L	Mass transfer coefficient (min^{-1})
MM	Solvent molar mass (g mol^{-1})
M_L	Mass of adsorbent (g)
Q	Flow rate (mL min^{-1})
q	Solid phase concentration (mg g^{-1})
q^*	Adsorption capacity (mg g^{-1})
$\bar{q}$	Average capacity in the solid phase (mg g^{-1})
q_m	Langmuir equation parameter, saturation capacity (mg g^{-1})
R	Radial coordinate
R_p	Particle radius (cm)
Re	Dimensionless Reynolds number
Sh	Dimensionless Sherwood number
Sc	Dimensionless Schmidt number
t	Time (min)
T	Absolute temperature (K)
v_s	Superficial velocity (cm min^{-1})
V_a	Molar volume at normal boiling point (cm^3 mol^{-1})
V_L	Packed bed volume(mL)
V_p	Total pore volume (cm^3)

V_s Solids volume (cm^3)
z Axial coordinate

Greek symbols
ε Bed porosity
ε_ρ Particle porosity
ρ_s Rock density (g cm^{-3})
φ Association coefficient
μ_b Solvent viscosity (cP)

1 Introduction

The method used to stimulate the oil production in the petroleum fields, is there water flooding, which is in offshore fields, where the seawater is injected into the wellbore (Sorbie and Mackay 2000; Bader 2006, 2007; Puntervold and Austad 2008; Binmerdhah et al. 2010).

The seawater injected is rich in sulfate ions and the formation water has barium, calcium, magnesium and strontium in high concentration, thus, forming insoluble sulfate salts when these waters are mixed (Bedrikovetsky et al. 2009; Senthilmurugan et al. 2011). Beyond sulfates and carbonates found, the aforesaid is formed by a pressure drop into the wellbore (Zhang and Dawe 1998; Zhang et al. 2001). These stated salts can be deposited in the production lines near the wellbore formations. This deposit block flow, promotes production loss and may deactivate all the production structure (Andrei and Gagliardi 2004; Martinod et al. 2008; Kumar et al. 2010; Vazquez et al. 2012). During the petroleum production, some factors intensify the scale formation, such as temperature, salinity and pressure (Xiaoyan et al. 2009; Bassioni 2010; Senthilmurugan et al. 2011; Reddy 2012).

Appling strong acids to decrease the pH and the quelant agents in order to do a complex with Ca^{2+} are to be used to remove and to prevent scale formation, however it requires high investments and may damage the rock formation (Ketrane et al. 2009).

Therefore, the most used technology for the prevention of deposits, is the squeeze treatment, which is the injection of a scale inhibitor into the wellbore and it may be adsorbed or precipitated as a complex in the rock surface (Rabaioli and Lockhart 1996; Andrei and Gagliardi 2004). The adsorption is a retention mechanism that is more convenient since the material deposition is minimized (Tantayakom et al. 2005).

In our laboratory, coreflood tests simulate the wellbore conditions in order to study the interaction between cores and inhibitors. Damage in the rock is evaluated after the squeeze treatment, through a measuring permeability (Ochi and Vernoux 1998; Rocha et al. 2004; Baraka-Lokmane and Sorbie 2010). However, in these said tests, the rock is confined under a high pressure and a brine used as seawater.

The inhibitors are chemical products that may do difficulties to the scale growth and reduce their adherence in the rock formation (Ketrane et al. 2009; Shen et al. 2012). The scale inhibitors most used are the acids of the phosphonic type, as methylenephosphonic acid, studied by Dyer and Graham (2003), Ketrane et al. (2009) and Baraka-Lokmane and Sorbie (Baraka-Lokmane and Sorbie 2010).

Two kinetic models were used to represent and to simulate the adsorption processes, as well as to estimate the mass transfer parameters. The selected models, such as the Linear Drive Force and the General Rate (GR) models, have been widely used to simulate several adsorption processes, such as (Santacesaria et al. 1982), Liu et al. (2010), Dantas et al. (2011a), Dantas et al. (2011b) and Luna et al. (2011). These said models were chosen for this particular study, due to the remarkable agreement in the modeling of the adsorption phenomena.

The purpose of this study is to evaluate the interactions between the core and the methylenephosphonic inhibitor (commercial product), through the column experiments in different concentrations and temperatures, as well as applying mathematical models in the adsorption data. Furthermore, the aforementioned models were used to evaluate the desorption profile using the estimated mass transfer parameters, since the squeeze yield depends on the desorption profile.

2 Experimental and modeling

2.1 Materials

Adsorption tests were evaluated using particles of the sandstone rock (about 90 % SiO_2) with 605 μm of a medium diameter. The commercial inhibitor used in the tests has about 17 % of aminomethylenephosphonic acid, as the active phase. The materials used in these studies were provided by Petrobras (Brazil). The interaction between rock and inhibitor was evaluated without presence of salts to reduce external factors in the adsorption process.

In order to analyze the samples after the adsorption test in the column experiments, Argon (purity >99 %) was used, which was supplied by White Martins Praxair Inc. and the phosphorus standard solution SpecSol of 1,000 mg L^{-1} supplied by Quimlab (Brazil). For determining the bulk density of the rock, the Helium (purity >99 %) was used.

2.2 Methods

2.2.1 Rock sandstone characterization

The rock was characterized by the N_2 isotherms at 77 K, in order to determinate the textural properties in surface area

and the total pore volume, measured in the Autosorb (Quantachrome, USA). The surface area was calculated using the BET methodology. Whereas the total pore volume was obtained from the N_2 volume adsorbed at a relative pressure of 0.95. Specific volume of solids was determined by experiments with Helium in a magnetic suspension balance (Rubotherm Bochum, Germany). Further details may be found in Dreisbach et al. (2002). The specific volume was used to determine the particle porosity (Eq. 1).

$$\varepsilon_p = \frac{v_p}{v_p + v_s}. \tag{1}$$

where ε_p is the particle porosity, V_s is the specific volume of solids (cm^3) and V_p is the total pore volume (cm^3).

2.2.2 Analytic method

Inductively coupled plasma optical emission spectrometry (ICP-OES, Thermo Scientific, USA) was used to determinate the inhibitor concentration during the column experiments. Argon was used in this equipment, in order to keep the inert atmosphere required for the tests, while the Phosphorus was the tracer used to determine the inhibitor concentration and the calibration in the analysis conditions shown on Table 1.

2.2.3 Column experiments

The interaction between the rock and the inhibitor was evaluated using a fixed bed experiments. The experimental apparatus consists of a steel column with 0.46 cm in diameter and 25 cm in length. The column was coupled to pump the system ProStar 210 Varian (USA) and the oven Eldex Laboratories CH-150 (USA).

The scale inhibitor solutions used in the adsorption test were prepared with the deionized water and pumped into the column, previously stabilized with the same deionized water. The feed concentration of 1–10 mg mL^{-1} with a flow rate of 0.1 mL min^{-1} at 30, 50 and 80 °C.

The bed porosity (ε) was determined by Eq. 2.

$$\varepsilon = 1 - \frac{M_L}{V_L \rho_S}. \tag{2}$$

where M_L is the mass of adsorbent (g), V_L is packed bed volume (mL) and ρ_s is the rock density (g cm^{-3}).

Table 1 Calibration and analysis conditions applied in ICP-OES of Thermo Scientific iCAP 6000 SERIES to phosphorus determination

Parameter	Values
Wavelength (nm)	213.618
Nebulizer	V-Groove (Babington)
Plasma power (W)	1,150
Gas nebulizer flow (L min^{-1})	2.45
Gas auxiliary flow (L min^{-1})	0.5

The adsorption capacity q^* was calculated through an integral mass balance from the breakthrough experiments in the column using Eq. 3, in which the flow was considered distributed equally in transversal section.

$$q* = \frac{C_0}{M_L}\left[Q\int\left(1 - \frac{C}{C_0}\right)dt - \varepsilon V_L\right]. \tag{3}$$

where q^* is the adsorption capacity (mg g^{-1}), C_0 is the initial concentration (mg mL^{-1}), C is the bulk liquid phase concentration (mg mL^{-1}), Q is the flow rate (mL min^{-1}).

Isotherms data experiments were treated using Langmuir equation (Eq. 4).

$$\frac{q*}{q_m} = \frac{bC_{eq}}{1 + bC_{eq}}. \tag{4}$$

where q_m and b are adjustment parameters that represent the saturation capacity (mg g^{-1}) and affinity adsorbate/adsorbent (mL mg^{-1}), respectively, and C_{eq} is the concentration in equilibrium in the liquid phase (mg mL^{-1}).

Desorption experiments were performed during 4 h, in order to evaluate the retention capacity of the inhibitor in the system. The same conditions of flow and temperature were maintained in these experiments. After each cycle of adsorption–desorption, the bed was washed with deionized water at 80 °C for 4 h at high flow rate (2 mL min^{-1}).

2.2.4 Modeling and estimation of mass transfer parameters

The linear driving force (LDF) and the GR models were used to simulate the adsorption processes and estimate the mass transfer parameters. The initial and boundary conditions applied in this work are normally applied to fixed bed adsorption processes (Santacesaria et al. 1982; Liu et al. 2010; Dantas et al. 2011a, 2011b). These parameters were used as input to the desorption simulations.

The LDF model is represented by Eqs. 5 and 6, in which the driving force for the mass transfer is the concentration gradient in the solid phase (Ruthven 1984).

Differential mass balance in liquid phase

$$\varepsilon\frac{\partial C(z,t)}{\partial t} + \rho_s(1-\varepsilon)\frac{\partial \bar{q}(z,t)}{\partial t} + v_s\frac{\partial C(z,t)}{\partial z} - \varepsilon.D_{ax}\frac{\partial^2 C(z,t)}{\partial z^2} = 0. \tag{5}$$

Differential mass balance in solid phase

$$\frac{\partial \bar{q}(z,t)}{\partial t} = K_L[q*(z,t) - \bar{q}(z,t)]. \tag{6}$$

where C is the bulk liquid phase concentration (mg mL^{-1}), $\bar{q}$ is the average capacity in the solid phase (mg g^{-1}), D_{ax} is

the axial dispersion coefficient ($cm^2\ min^{-1}$), v_s is the superficial velocity ($cm\ min^{-1}$) and K_L is the mass transfer coefficient (min^{-1}).

The initial and the boundary conditions used are expressed in Eqs. 7–10. These conditions were based on the dynamic flow in the column, whereas the mass transfer was based in the axial direction.

Initial conditions

$$t = 0 \qquad C(z,0) = 0 \tag{7}$$

$$q(z,0) = 0. \tag{8}$$

Boundary conditions

$$z = 0 \qquad \frac{\partial C(0,t)}{\partial z} = \frac{v_s}{\varepsilon . D_{ax}}[C(0,t) - C_0] \tag{9}$$

$$z = L \qquad \frac{\partial C(L,t)}{\partial z} = 0. \tag{10}$$

To simulate the desorption curves, the initial and boundary conditions that were used are expressed in Eqs. 11–14. The concentration in the liquid phase is the feed concentration of the adsorption process, due to the fact that the bed is saturated. In the solid phase, the concentration is the adsorbed amount as given by the equilibrium equation.

Initial conditions

$$t = 0 \qquad C(z,0) = C_0 \tag{11}$$

$$q(z,0) = \frac{q_m b C_0}{1 + bC_0}. \tag{12}$$

Boundary conditions

$$z = 0 \qquad \frac{\partial C(0,t)}{\partial z} = \frac{v_s . C(0,t)}{\varepsilon . D_{ax}} \tag{13}$$

$$z = L \qquad \frac{\partial C(L,t)}{\partial z} = 0. \tag{14}$$

In the GR model, internal and external resistances to the mass transfer influenced the kinetic behavior in the fixed bed adsorption system. The model consists of the adsorbate mass balance in the liquid (Eq. 15) and the solid phase (Eq. 20), followed by the initial (Eqs. 16, 17 and 21), as well as the boundary (Eqs. 18, 19, 22 and 23) conditions (Santacesaria et al. 1982; Liu et al. 2010).

Differential mass balance in liquid phase

$$\varepsilon \frac{\partial C(z,t)}{\partial t} + v_s \frac{\partial C(z,t)}{\partial z} = \varepsilon . D_{ax} \frac{\partial^2 C(z,t)}{\partial z^2} - (1 - \varepsilon) . \frac{3k_f}{R_p}\left[C(z,t) - C_p(R_p,t)\right]. \tag{15}$$

Initial conditions

$$t = 0 \qquad C(z,0) = 0 \tag{16}$$

$$C_p(R,0) = 0. \tag{17}$$

Boundary conditions

$$z = 0 \qquad v_s . C(0,t) - D_{ax} \frac{\partial C(0,t)}{\partial z} = v_s . C_0 \tag{18}$$

$$z = L \qquad \frac{\partial C(L,t)}{\partial z} = 0. \tag{19}$$

Differential mass balance in solid phase

$$\varepsilon_p \frac{\partial C_p(R,t)}{\partial t} + \rho_s (1 - \varepsilon_p) \frac{\partial q(R,t)}{\partial t} = \frac{D_p}{R^2} \frac{\partial}{\partial R}\left(R^2 \frac{\partial C_p(R,t)}{\partial R}\right). \tag{20}$$

Initial condition

$$t = 0 \qquad q(R,0) = 0. \tag{21}$$

Boundary conditions

$$R = 0 \qquad \frac{\partial q(0,t)}{\partial R} = \frac{\partial C_p(0,t)}{\partial R} = 0 \tag{22}$$

$$R = R_p \qquad D_p \frac{\partial C_p(R_p,t)}{\partial R} = k_f[C(z,t) - C_p(R_p,t)] \tag{23}$$

where C_p is the intra-particle liquid phase concentration ($mg\ mL^{-1}$), q is a function of C_p calculated from the Langmuir equation, k_f is the film mass transfer coefficient ($cm\ min^{-1}$), D_p is the pore diffusion coefficient ($cm^2\ min^{-1}$) and R_p is particle radius (cm).

To simulate the desorption curves to the GR model, the initial and the boundary conditions used are expressed in the Eqs. 24–28.

Initial conditions

$$t = 0 \qquad C(z,0) = C_0 \tag{24}$$

$$C_p(R,0) = C_0 \tag{25}$$

$$q(R,0) = \frac{q_m b C_0}{1 + bC_0}. \tag{26}$$

Boundary conditions

$$z = 0 \qquad v_s . C(0,t) = D_{ax} \frac{\partial C(0,t)}{\partial z} \tag{27}$$

$$z = L \qquad \frac{\partial C(L,t)}{\partial z} = 0. \tag{28}$$

The axial dispersion coefficient D_{ax} was estimated from the correlation, using Peclet and Reynolds numbers (Butt 1980), as shown in the Eq. 29 (Santacesaria et al. 1982).

$$\varepsilon \frac{D_{ax}}{v_s d_p} = 0.2 + 0.011 \mathrm{Re}^{0.48}. \tag{29}$$

where d_p is the average particle diameter (cm).

The external mass transfer coefficient was estimated from the Geankoplis-Wilson equation (Eq. 30), which is valid for the liquid phase (Ruthven 1984).

$$Sh = \frac{d_p k_f}{D_m} = \frac{1.09}{\varepsilon}(Sc)^{1/3}(\mathrm{Re})^{1/3}, \quad (30)$$

where D_m is the molecular diffusivity coefficient (cm^2 min^{-1}) and Sc is the Schmidt number.

The molecular diffusion coefficient (D_m) of scale inhibitor was calculated using the Wilke and Chang correlation, expressed in Eq. 31 (Wilke and Chang 1955).

$$D_m = 7.48 \times 10^{-8}\left[\frac{(MM.\varphi)^{0.5}.T}{\mu_{B.}V_a^{0.6}}\right], \quad (31)$$

where MM is the solvent molar mass (g mol^{-1}), φ is the association coefficient, T is the temperature (K), μ_b is the solvent viscosity (cP) and V_a is the molar volume at boiling point (cm^3 mol^{-1}).

The coefficients K_L and D_p were estimated using heterocedastic estimation method of the computational package gPROMS, within the limits specified in simulation and using experimental data. The computational package used the method of orthogonal collocation on finite elements (OCFEM) with 6 sections and 3 collocation points, has been applied to the fixed bed adsorption processes by Kaczmarski et al. (1997), Liu et al. (2010) and Luna et al. (2011).

3 Results and discussion

3.1 Rock characterization

The profile of the N_2 isotherms (Fig. 1), showed that the sandstone rock used has a low porosity, being a characteristic of the isotherm type III, according to the BDDT classification (Thomas and Crittenden 1998). The textural parameters of the sandstone rock are reported on Table 2.

It has been observed that the rock particles used in this study had a low porosity, surface area and a pore volume. As expected, the core porosity was about 20 % (Baraka-Lokmane et al. 2009), which was resulted from the adjustment of the rock fragments, during its formation. Therefore, the defragmentation resulted in the low porosity particles.

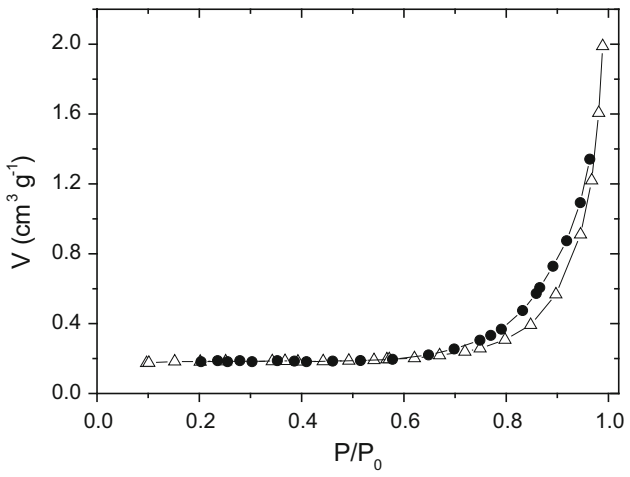

Fig. 1 N_2 (*white triangle*) adsorption and (*filled circle*) desorption isotherms at 77 K of sandstone rock

Table 2 Textural properties of the rock particles

Parameter	Values
S_{BET} (m^2 g^{-1})	0.51
V_p (cm^3 g^{-1})	3.08×10^{-3}
ρ_s (g cm^{-3})	2.66
V_s (cm^3)	0.45
ε_p	0.0068

Table 3 Fixed bed characteristics

Properties	Results
V_L (cm^3)	4.155
ε	0.57
D_{ax} (cm^2 min^{-1})	0.178

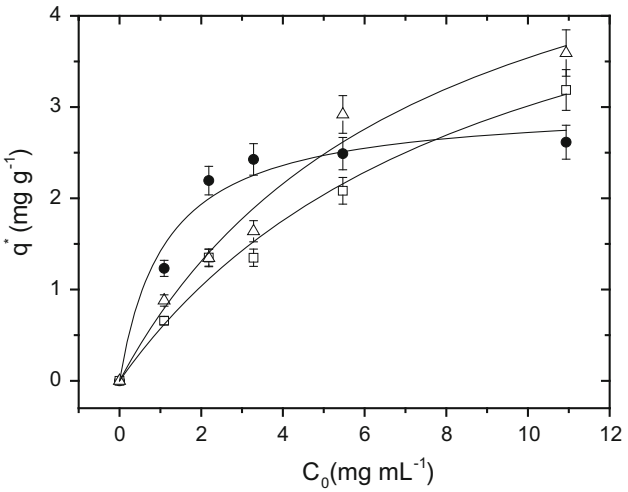

Fig. 2 Adsorption isotherms of scale inhibitor at (*white square*) 30 °C, (*filled circle*) 50 °C and (*white triangle*) 80 °C. Isotherms fit by (*solid line*) Langmuir equation

Table 4 Parameters of Langmuir equation

Parameter	30 °C	50 °C	80 °C
q_m (mg g^{-1})	5.75 ± 0.92	3.03 ± 0.24	6.17 ± 0.971
b (mL mg^{-1})	0.11 ± 0.03	0.88 ± 0.28	0.135 ± 0.039
R^2	0.98	0.97	0.98
χ^2	0.024	0.038	0.043

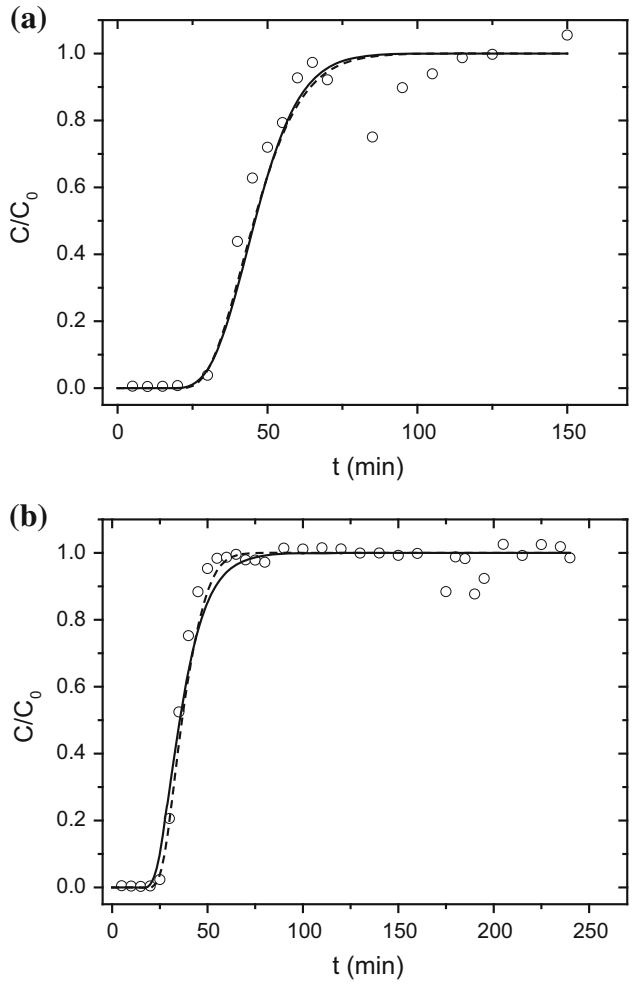

Fig. 3 Experimental and simulated breakthrough curves by (*solid line*) LDF and (*dashed line*) GR models at 30 °C at **a** 1 mg mL^{-1} and **b** 10 mg mL^{-1}

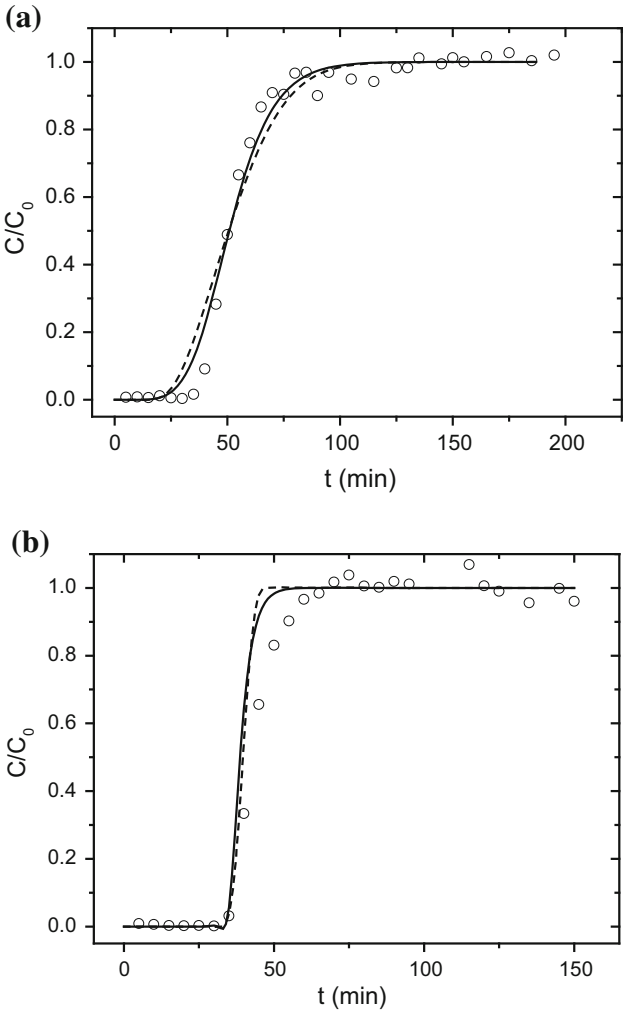

Fig. 4 Experimental and simulated breakthrough curves by (*solid line*) LDF and (*dashed line*) GR models at 50 °C at **a** 1 mg mL^{-1} and **b** 10 mg mL^{-1}

3.2 Column experiments

The column was uniformly packed with fragmented rock and the properties are shown on Table 3.

The isotherm data obtained in the column experiments were plotted in Fig. 2, for each feed concentration, with the adsorption capacity from mass balance. On Table 4, the estimated parameters of the Langmuir equation for each isotherm were reported.

In the physisorption, usually the capacity adsorption decreases with increasing temperature. However, in the experimental data with the temperature rising from 30 to 80 °C, the adsorption capacity increased by 7 %, following a different profile, thus, suggesting that other phenomena occurred to promote interaction between the rock and the inhibitor. These interactions may be attributed to electrostatic changes in the rock surface, as observed in other studies with silica materials (Jada et al., 2006; Waseem et al., 2011). Electrostatic modifications phenomena in silica materials were also observed by Waseem et al. (2011) for adsorption of Cd (II) on SiO_2, where metal adsorption capacity increased from 0.033 to 0.043 mmol g^{-1} with increasing temperature. Jada et al. (2006) obtained the same behavior in adsorption experiments with quartz sand.

3.3 Modeling and estimation of mass transfer parameters

In Figs. 3, 4 and 5, the experimental and simulated breakthrough curves at 30, 50 and 80 °C, are shown.

There was a good agreement between the experimental data and the curves obtained from the simulations, therefore, confirming that the models employed were generating good predictions in the concentration profiles of the outlet in the column.

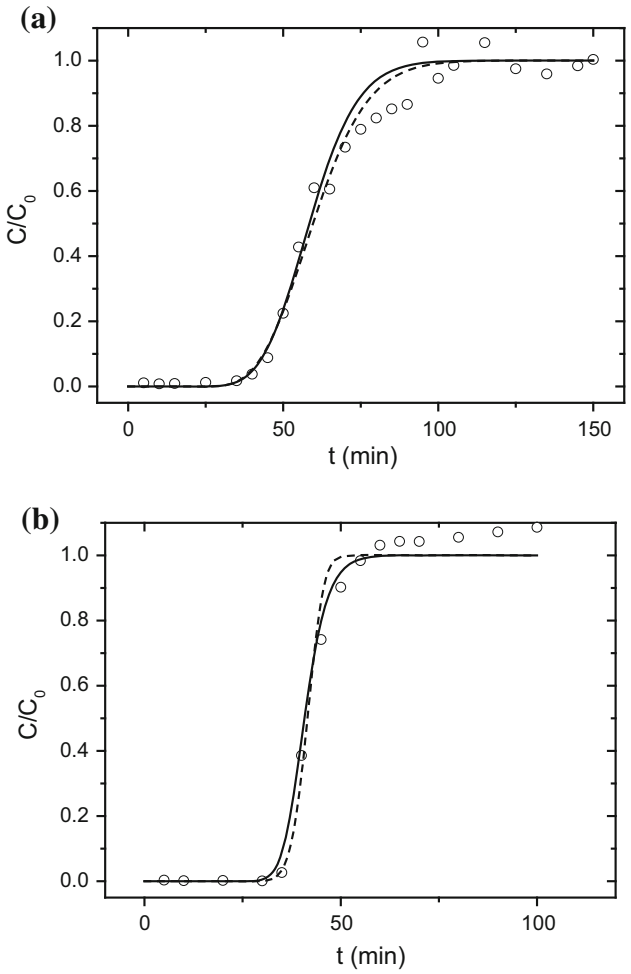

Fig. 5 Experimental and simulated breakthrough curves by (*solid line*) LDF and (*dashed line*) GR models at 80 °C at **a** 1 mg mL^{-1} and **b** 10 mg mL^{-1}

The mass transfer parameters, K_L estimated by the LDF model and D_p estimated by the GR model, are shown on Table 5.

The estimated D_p, using the GR model was very low. Thus, showing a high diffusion resistance. These hypotheses are consequences of the very low porosity in the particles. The parameters K_L and D_p, which represent the mass transfer resistance and the intraparticle diffusion, respectively, at concentration range of 1.0–10.0 mg mL^{-1}, showed a low variance. However, when the parameters are observed at the same concentration with a temperature increase, the K_L and D_p presented a slight tendency to increase.

Desorption curves were simulated, using the mass transfer parameters obtained from both models with the adsorption data. In Fig. 6 and 7, the experimental and simulated curves at 30 and 80 °C are shown.

The simulation at 1.0 and 2.0 mg mL^{-1} showed low agreement with the experimental data. Probably, part of the inhibitor fed to the column still remained in the system after 4 h. The differences between the areas above the adsorption curves and below the desorption curves are shown in Table 6.

The areas above the adsorption curve and below the desorption curve are different at 1.0 and 2.0 mg mL^{-1} to 30 and 80 °C experiments, showing that inhibitor was still in the system, in the liquid or solid phase, after 4 h of elution. This behavior is expected in the squeeze treatment to expand the lifetime, because the inhibitor remains in contact with the rock for a longer period time in the wellbore. However, at 10.0 mg mL^{-1}, it was observed that almost all inhibitor was eluted. In this case, desorption may be favored by temperature increase.

Table 5 Estimated mass transfer parameters

			LDF	GR	
T (°C)	C_0 (mg mL^{-1})	D_m (cm^2 min^{-1})	K_L (min^{-1})	k_f (cm min^{-1})	D_p (cm^2 min^{-1})
30	1.0	2.57×10^{-4}	0.34	5.14×10^{-2}	2.55×10^{-5}
	2.0		0.58		5.25×10^{-5}
	3.0		0.26		1.23×10^{-5}
	5.0		0.25		1.05×10^{-5}
	10.0		0.13		9.81×10^{-6}
50	1.0	4.02×10^{-4}	0.16	6.92×10^{-2}	1.62×10^{-5}
	2.0		0.12		3.20×10^{-5}
	3.0		0.15		1.90×10^{-5}
	5.0		0.30		5.38×10^{-5}
	10.0		0.36		3.31×10^{-5}
80	1.0	6.82×10^{-4}	0.44	9.84×10^{-2}	4.90×10^{-5}
	2.0		0.67		7.89×10^{-5}
	3.0		0.77		8.13×10^{-5}
	5.0		0.93		9.78×10^{-5}
	10.0		0.56		6.91×10^{-5}

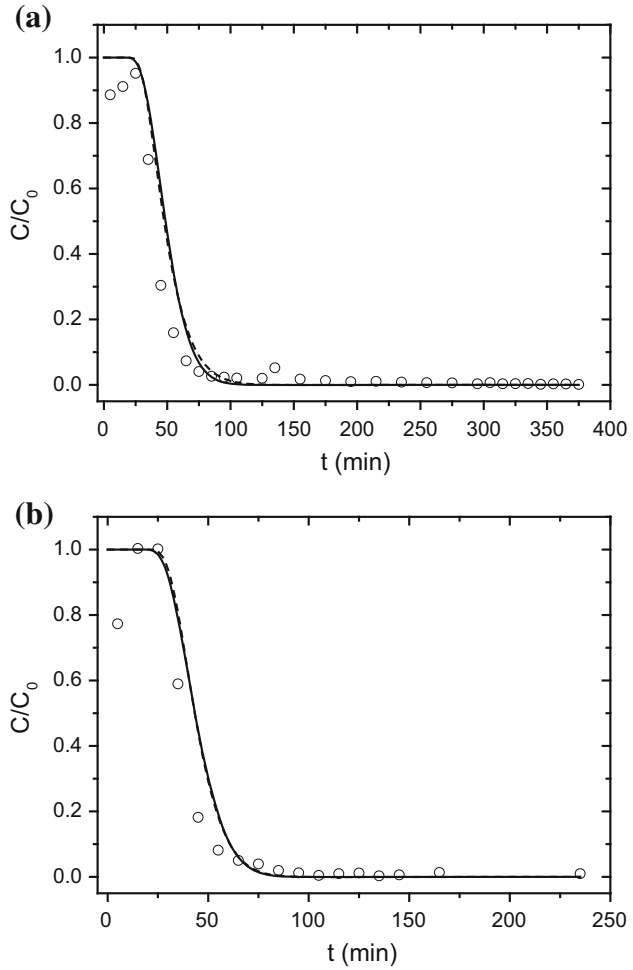

Fig. 6 Experimental and simulated breakthrough curves by (*solid line*) LDF and (*dashed line*) GR models at 30 °C at (**a**) 1 mg mL^{-1} and (**b**) 2 mg mL^{-1}

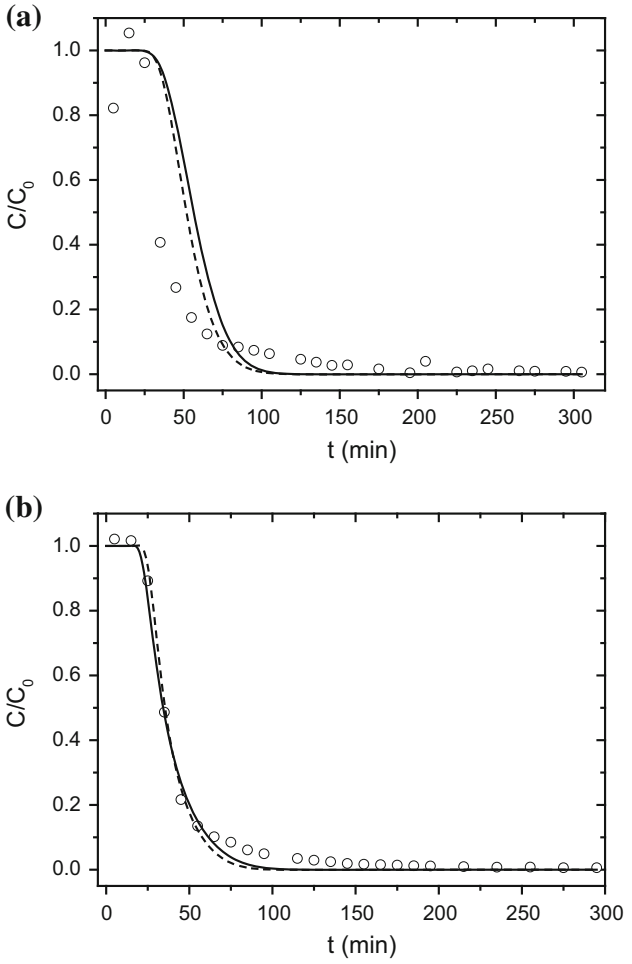

Fig. 7 Experimental and simulated breakthrough curves by (*solid line*) LDF and (*dashed line*) GR models at 80 °C at (**a**) 1 mg mL^{-1} and (**b**) 10 mg mL^{-1}

Table 6 Areas above the breakthrough curves and below the desorption curves

Experiments	Areas (min)		Difference (%)
	Adsorption	Desorption after 4 h	
C = 1.0 mg mL^{-1} at 30 °C	52.66	42.45	19.1
C = 2.0 mg mL^{-1} at 30 °C	53.38	35.01	34.4
C = 1.0 mg mL^{-1} at 80 °C	62.40	41.77	33.1
C = 10.0 mg mL^{-1} at 80 °C	39.48	38.37	2.8

4 Conclusion

Adsorption of the commercial scale inhibitor on sandstone rock was studied using column experiments. The kinetic models were used to simulate experimental data and the estimated mass transfer parameters were applied to simulate the desorption curves.

The isotherms were measured from the mass balance in the breakthrough curves and the Langmuir equation was used to fit the experimental data with a remarkable agreement.

The LDF and GR models were able to represent the adsorption process of the inhibitor on the sandstone rock in the column experiments. The estimated K_L and D_p using the model showed a slight tendency, at the same concentration, to increase with increasing temperature.

We believe these stated models would be used to properly estimate the physical phenomena occurring in the squeeze treatments of the petroleum industry.

Acknowledgments The financial and logistic support provided by CAPES (Coordenação de Aperfeiçoamento de Pessoal de Nível Superior), CNPq (Conselho Nacional de Pesquisa e Desenvolvimento Científico) and PETROBRAS (Petróleo Brasileiro S.A.).

References

Andrei, M., Gagliardi, F.: Redissolution studies in bulk and in coreflood for PPCA scales inhibitor. J. Pet. Sci. Eng. **43**, 35–55 (2004)

Bader, M.S.H.: Sulfate scale problems in oil fields water injection operations. Desalination **201**, 100–105 (2006)

Bader, M.S.H.: Sulfate removal technologies for oil fields seawater injection operations. J. Pet. Sci. Eng. **55**, 93–110 (2007)

Bassioni, G.: Mechanistic aspects on the influence of inorganic anion adsorption on oilfeld scale inhibition by citrate. J. Pet. Sci. Eng. **70**, 298–301 (2010)

Baraka-Lokmane, S., Sorbie, K.S.: Effect of pH and scale inhibitor concentration on phosphonate-carbonate interaction. J. Pet. Sci. Eng. **70**, 10–27 (2010)

Baraka-Lokmane, S., Main, I.G., Ngwenya, B.T., Elphick, S.C.: Application of complementary methods for more robust characterization of sandstone cores. Mar. Petrol. Geol. **26**, 39–56 (2009)

Bedrikovetsky, P., Silva, R.M.P., Daher, J.S., Gomes, J.A.T., Amorim, V.C.: Well-data-based prediction of productivity decline due to sulphate scaling. J. Pet. Sci. Eng. **68**, 60–70 (2009)

Binmerdhah, A.B., Yassin, A.A., Muherei, M.A.: Laboratory and prediction of barium sulfate scaling at high-barium formation water. J. Pet. Sci. Eng. **70**, 79–88 (2010)

Butt, J.B.: Reaction Kinetics and Reactor Design. Prentice Hall, Englewood Cliffs (1980)

Dantas, T.L.P., Luna, F.M.T., Silva Jr, I.J., de Azevedo, D.C.S., Grande, C.A., Rodrigues, A.E., Moreira, R.F.P.M.: Carbon dioxide-nitrogen separation through adsorption on activated carbon in a fixed bed. Chem. Eng. J. **169**, 11–19 (2011a)

Dantas, T.L.P., Luna, F.M.T., Silva Jr, I.J., Torres, A.E.B., de Azevedo, D.C.S., Rodrigues, A.E., Moreira, R.F.P.M.: Modeling of the fixed-bed adsorption of carbon dioxide and a carbon dioxide-nitrogen mixture on zeolite 13X. Braz. J. Chem. Eng. **28**, 533–544 (2011b)

Dreisbach, F., Losch, H.W., Harting, P.: Highest pressure adsorption equilibria data: measurement with magnetic suspension balance and analysis with a new adsorbent/adsorbate-volume. Adsorption **8**, 95–109 (2002)

Dyer, S.J., Graham, G.M.: Thermal stability of generic barium sulphate scale inhibitor species under static and dynamic conditions. J. Pet. Sci. Eng. **37**(3–4), 171–181 (2003)

Jada, A., AitAkbour, R., Douch, J.: Surface charge and adsorption from water onto quartz sand of humic acid. Chemosphere **64**, 1287–1295 (2006)

Kaczmarski, K., Mazzotti, M., Storti, G., Morbidelli, M.: Modeling fixed-bed adsorption columns through orthogonal collocations on moving finite elements. Comput. Chem. Eng. **21**(6), 641–660 (1997)

Ketrane, R., Saidani, B., Gil, O., Leleyter, L., Baraud, F.: Efficiency of five scale inhibitors on calcium carbonate precipitation from hard water: effect of temperature and concentration. Desalination **249**, 1397–1404 (2009)

Kumar, T., Vishwanatham, S., Kundu, S.S.: A laboratory study on pteroyl-L-glutamic acid as a scale prevention inhibitor of calcium carbonate in aqueous solution of synthetic produced water. J. Pet. Sci. Eng. **71**, 1–7 (2010)

Liu, B., Zeng, L., Mao, J., Ren, Q.: Simulation of levulinic acid adsorption in packed beds using parallel pore/surface diffusion model. Chem. Eng. Technol. **33**(7), 1146–1152 (2010)

Luna, F.M.T., Araújo, C.C.B., Veloso, C.B., Silva Jr, I.J., Azevedo, D.C.S., Cavalcante Jr, C.L.: Adsorption of naphthalene and pyrene from isooctane solutions on commercial activated carbons. Adsorption **17**, 937–947 (2011)

Martinod, A., Euvrard, M., Foissy, A., Neville, A.: Progressing the understanding of chemical inhibition of mineral scale by green inhibitors. Desalination **220**, 345–352 (2008)

Ochi, J., Vernoux, J.-F.: Permeability decrease in sandstone reservoirs by fluid injection—Hydrodynamic and chemical effects. J. Hydrol. **208**, 237–248 (1998)

Puntervold, T., Austad, T.: Injection of seawater and mixtures with produced water into North Sea chalk formation: impact of fluid-rock interactions on wettability and scale formation. J. Pet. Sci. Eng. **63**, 23–33 (2008)

Rabaioli, M.R., Lockhart, T.P.: Solubility and phase behavior of polyacrylate scale inhibitors. J. Pet. Sci. Eng. **15**, 115–126 (1996)

Reddy, M.M.: Calcite growth-rate inhibition by fulvic acid and magnesium ion-Possible influence on biogenic calcite formation. J. Cryst. Growth **352**, 151–154 (2012)

Rocha, A.A., Miekeley, N., Bezerra, M.C.M., Küchler, I.L.: An automated system for preconcentration/matrix-removal followed by ICP-MS determination of organic phosphorus in oil production water. Microchem. J. **78**, 65–70 (2004)

Ruthven, D.M.: Principles of Adsorption and Adsorption Processes. Wiley, New York (1984)

Santacesaria, E., Morbidelli, M., Servida, A., GIusepe, S., Carra, S.: Separation of xylenes on Y zeolites 2. Breakthrough curves and their interpretation. Ind. Chem. Proc. Desenv. Devlop **21**, 446–451 (1982)

Senthilmurugan, B., Ghosh, B., Sanker, S.: High performance maleic acid based oil well scale inhibitors—Development and comparative evaluation. J. Ind. Eng. Chem. **17**, 415–420 (2011)

Shen, Z., Li, J., Xu, K., Ding, L., Ren, H.: The effect of synthesized hydrolyzed polymaleic anhydride (HPMA) on the crystal of calcium carbonate. Desalination **284**, 238–244 (2012)

Sorbie, K.S., Mackay, E.J.: Mixing of injected, connate and aquifer brines in waterflooding and its relevance to oilfield scaling. J. Pet. Sci. Eng. **27**, 85–106 (2000)

Tantayakom, V., Fogler, H.S., Charoensirithavorn, P., Chavadej, S.: Kinetic study of scale inhibitor precipitation in squeeze treatment. Cryst. Growth Des. **5**(1), 329–335 (2005)

Thomas, W.J., Crittenden, B.: Adsorption Technology and Design. Elsevier Science & Technology, Amsterdam (1998)

Vazquez, O., Mackay, E., Sorbie, K.: A two-phase near-wellbore simulator to model non-aqueous scale inhibitor squeeze treatments. J. Pet. Sci. Eng. **82–83**, 90–99 (2012)

Waseem, M., Mustafa, S., Naeem, A., Shah, K.H., Shah, I.: Mechanism of Cd (II) sorption on silica synthesized by sol-gel method. Chem. Eng. J. **169**, 78–83 (2011)

Wilke, C.R., Chang, P.: Correlation of diffusion coefficients in dilute solution. AIChE J. **1**(2), 264–270 (1955)

Xiaoyan, L., Jungang, L., Qianya, Z., Jinlai, F., Yingli, L., Jingxin, S.: The analysis and prediction of scale accumulation for water-injection pipelines. J. Pet. Sci. Eng. **66**, 161–164 (2009)

Zhang, Y., Dawe, R.: The kinetics of calcite precipitation from a high salinity water. Appl. Geochem. **13**, 177–184 (1998)

Zhang, Y., Shaw, H., Farquhar, R., Dawe, R.: The kinetics of carbonate scaling—application for the prediction. J. Pet. Sci. Eng. **29**, 85–95 (2001)